

Article

Properties of Mn^{2+} and π -Electron Spin Systems Probed by 1H and ^{13}C NMR in the Organic Conductor κ -(BETS) $_2Mn[N(CN)_2]_3$

Oleg M. Vyaselev ^{1,*}, Reizo Kato ², Hiroshi M. Yamamoto ², Megumi Kobayashi ²,
Leokadiya V. Zorina ¹, Sergey V. Simonov ¹, Nataliya D. Kushch ³ and Eduard B. Yagubskii ³

¹ Institute of Solid State Physics, Russian Academy of Sciences, Chernogolovka, Moscow region, 142432, Russia; E-Mails: zorina@issp.ac.ru (L.V.Z.), simonovsv@rambler.ru (S.V.S.)

² Institute of Physical and Chemical Research (RIKEN), Hirosawa, Wako, Saitama 351-0198, Japan; E-Mails: reizo@riken.jp (R.K.); yhiroshi@riken.jp (H.M.Y.); kobame@riken.jp (M.K.)

³ Institute of Problems of Chemical Physics, Russian Academy of Sciences, Chernogolovka, Moscow region, 142432, Russia; E-Mails: kushch@icp.ac.ru (N.D.K.); yagubski@icp.ac.ru (E.B.Y.)

* Author to whom correspondence should be addressed; E-Mail: vyasel@issp.ac.ru;
Tel.: +7-49652-28374; Fax: +7-49652-28160.

Received: 7 March 2012; in revised form: 30 March 2012 / Accepted: 31 March 2012 /

Published: 12 April 2012

Abstract: Properties of the spin systems of the localized $3d Mn^{2+}$ ions and the conduction π electrons in quasi-two-dimensional organic conductor κ -(BETS) $_2Mn[N(CN)_2]_3$ were accessed using 1H and ^{13}C NMR in order to find their relation to the metal-insulator transition which occurs at ~ 23 K. The transition of the system into the insulating state is shown to be followed by localization of the π spins into a long-range ordered staggered structure of AF type. In contrast, the $3d Mn^{2+}$ electron spin moments form a disordered tilted structure, which may signify their trend to AF order, frustrated geometrically by the triangular arrangement of Mn in the anion layer. This result suggests that the MI transition in κ -(BETS) $_2Mn[N(CN)_2]_3$ is not the consequence of the interactions within the Mn^{2+} spins but due to the interactions within the π -electron system itself. Vice versa, it is more likely that the disordered tilted structure of the Mn^{2+} spins is induced by the ordered π -spins via the π - d interaction.

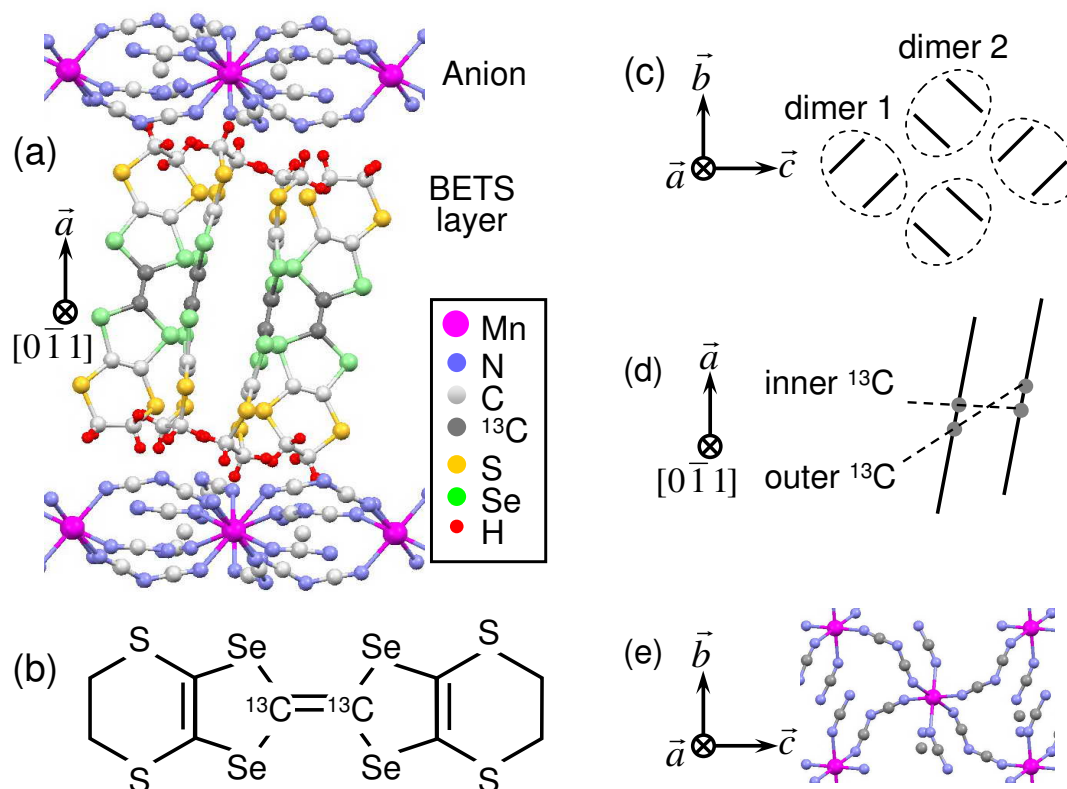
Keywords: organic metals; π - d interactions; spin order; antiferromagnetism; metal-insulator transition; NMR

PACS Classification: 74.70.Kn; 71.30.+h; 76.60.Jx; 75.30.-m

1. Introduction

NMR is a versatile tool for local-level investigation of magnetic properties in complex molecular systems. This technique uses nuclear spins to spy on the electron spin system by monitoring the local magnetic field created by electron spins at the nucleus site. Since NMR frequency is nucleus-specific, the experiment tuned to particular nucleus probes the electron spin system at the site of the corresponding atom within the crystal structure. In complex compounds incorporating more than one electron spin system (e.g., itinerant and localized electrons) such information helps to discriminate between the events developing within the electron subsystems and determine the interrelation between them.

Figure 1. (a) Side view (along $[0\bar{1}1]$) of crystal structure of κ -(BETS) $_2$ Mn[N(CN) $_2$] $_3$; (b) BETS molecule with ^{13}C in positions of the central C=C bond; (c) Top view of schematic crystal structure of the conducting BETS layer. The circled pairs of lines represent (BETS) $_2$ dimers; (d) Side view of BETS dimer with site definition of the central C=C carbons; (e) Top view of the anion layer.



The quasi-two-dimensional organic conductor κ -(BETS) $_2$ Mn[N(CN) $_2$] $_3$ (BETS = C $_{10}$ S $_4$ Se $_4$ H $_8$, *bis*-(ethylenedithio)tetraselenafulvalene) is an example of such compound (Figure 1). The system is metallic down to $T_{\text{MI}} \sim 23$ K where it undergoes the metal-insulator (MI) transition [1,2]. Its

conductivity is associated with π -electrons confined within the layers of dimerised organic BETS molecules, sandwiched between the insulating polymeric $\text{Mn}[\text{N}(\text{CN})_2]_3$ anion layers, while the bulk magnetization is determined by Mn^{2+} ($J = S = 5/2, L = 0$) ions of the anion layers [3]. The static susceptibility in the metallic state is isotropic and obeys accurately the Curie–Weiss law. Below T_{MI} it becomes slightly smaller than the Curie–Weiss value, $\chi_{\text{CW}}(T)$, so that at $T = 2$ K it makes 80%–85% of χ_{CW} , still essentially isotropic. This trend suggests that below T_{MI} the Mn^{2+} system tends towards antiferromagnetic (AF) order, which is however frustrated geometrically by triangular arrangement of Mn in the anion layer (Figure 1e). In the akin compound λ -(BETS) $_2\text{FeCl}_4$ with rectangular network of FeCl_4 units, the susceptibility governed by Fe^{3+} moments demonstrates below $T_{\text{MI}} = 8$ K the distinctive features characteristic of a uniaxial Néel-type antiferromagnet with $T_N = T_{\text{MI}}$, which gave grounds to nominate the AF ordering within Fe^{3+} ions as driving force of the MI transition [4]. One can assume therefore that the AF interaction within the Mn^{2+} d -electron spins in the title compound may in a similar way cause localization of the conduction π electrons at T_{MI} due to strong π - d coupling presumably present in the system [5].

On the other hand, the MI transition is not only specific to quasi-two-dimensional organic conductors with magnetic anions: there are known non-magnetic compounds where the insulating state is attributed to strong electron correlations within the half-filled conducting band leading to Mott instability and electron localization [6]. Moreover, in some of them the electrons localize into the long-range AF structure (e.g., κ -(ET) $_2\text{Cu}[\text{N}(\text{CN})_2]\text{Cl}$ [7], β' -(ET) $_2\text{X}$ ($\text{X} = \text{ICl}_2, \text{AuCl}_2$) [8], where ET is isostructural to BETS but with sulphur on Se sites). Besides, recent experiments on λ -(BETS) $_2\text{FeCl}_4$ [9,10] have doubted the AF order in the Fe^{3+} spin system and its responsibility for the MI transition, stating that it is the π -electron system that orders antiferromagnetically and produces the MI transition, while the Fe^{3+} d -electrons remain in the paramagnetic state.

There is therefore a question if the magnetic interactions within Mn^{2+} moments in κ -(BETS) $_2\text{Mn}[\text{N}(\text{CN})_2]_3$ are responsible for the MI transition, or it is a domestic affair of the conduction electrons as in some non-magnetic quasi-two-dimensional systems. To address this issue we have performed ^1H and ^{13}C NMR measurements on κ -(BETS) $_2\text{Mn}[\text{N}(\text{CN})_2]_3$ single crystals. For ^{13}C NMR, the crystal with BETS molecules containing >99% of ^{13}C isotope in the central C=C bond (Figure 1b) was used. Hydrogen atoms belonging to the ethylene groups at the terminals of BETS molecules (Figure 1a) are relatively close to the Mn sites and therefore are expected to provide information about the Mn^{2+} subsystem through dipolar fields induced by Mn^{2+} moments at hydrogen sites. ^{13}C NMR on the carbons from the central C=C bond of the BETS molecule is known to be effective in probing the conduction π -electron spin system [11]. The two experiments combined together promise the complete description of the magnetic properties of the system.

2. Results and Discussion

2.1. ^1H NMR

Hydrogen sites located at the terminals of BETS molecules (Figure 1a) have negligibly small hyperfine coupling with conduction electrons [12], therefore the NMR frequency shift should be determined by the dipolar fields from the $3d$ Mn^{2+} ion electron spin moments ($S_d = 5/2, g \approx 2$).

For the arbitrary orientation of the magnetic field, the ^1H NMR spectrum will count 16 peaks: there are 8 inequivalent crystallographic hydrogen sites and two magnetically inequivalent orientations of the BETS dimer (Figure 1c). The BETS molecules within the dimer are inversion-symmetric to each other, thus magnetically equivalent.

Figure 2 shows ^1H NMR spectrum in $\kappa\text{-(BETS)}_2\text{Mn}[\text{N}(\text{CN})_2]_3$ at $T = 74$ K in field $H_0 = 7$ T oriented at $\theta = 22^\circ$ from \vec{a}^* towards $[00\bar{1}] (= -\vec{c})$ direction. The spectrum is shown with respect to $^1\nu_0 = ^1\gamma H_0$, where $^1\gamma = 42.5759$ MHz/T is the proton gyromagnetic ratio. For the chosen geometry ($\vec{H} \perp \vec{b}$), the two different orientations of the BETS dimer shown in Figure 1c become magnetically equivalent which reduces the total number of peaks to 8. Arrows in Figure 2 indicate the 8 peaks.

Figure 2. ^1H NMR spectrum in $\kappa\text{-(BETS)}_2\text{Mn}[\text{N}(\text{CN})_2]_3$ at $T = 74$ K in field $H_0 = 7$ T oriented at $\theta = 22^\circ$ from \vec{a}^* towards $[00\bar{1}] (= -\vec{c})$ direction. The spectrum is shown with respect to $^1\nu_0 = ^1\gamma H_0$.

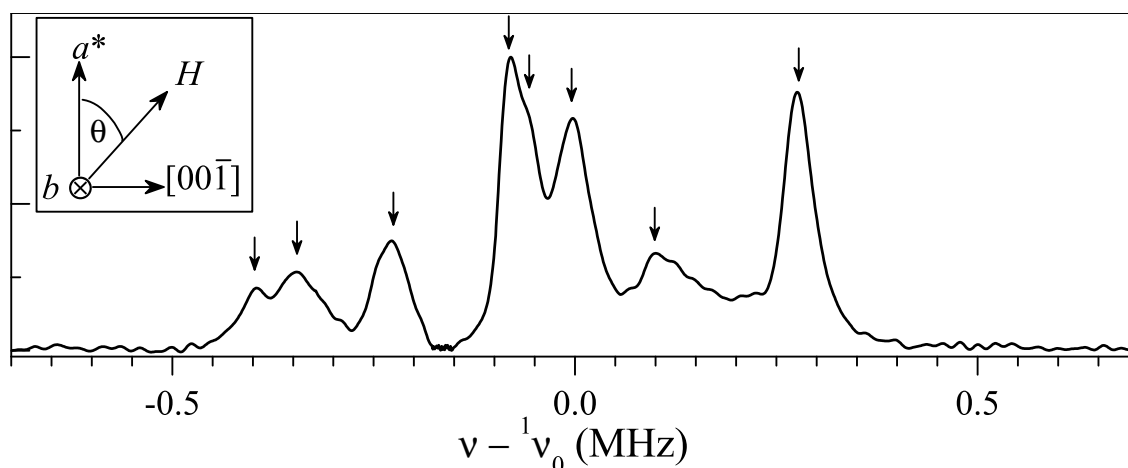
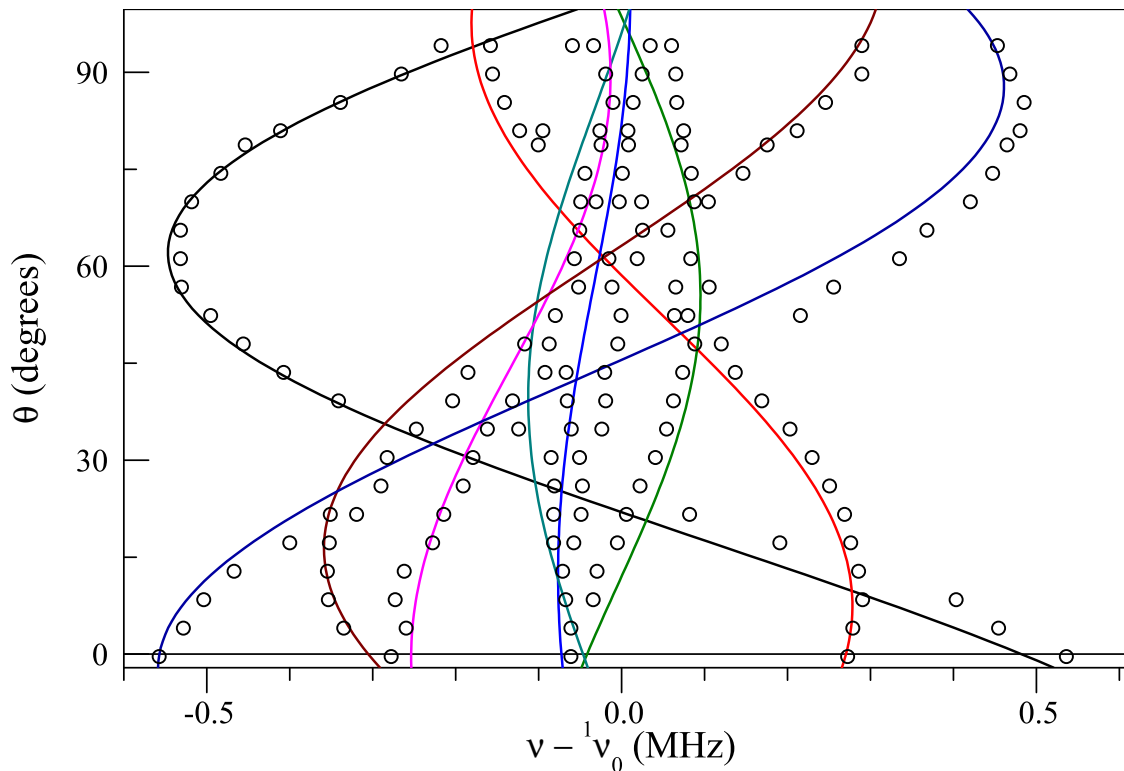


Figure 3 presents the angular evolution of ^1H NMR peak positions in $\kappa\text{-(BETS)}_2\text{Mn}[\text{N}(\text{CN})_2]_3$ measured at 74 K in field $H_0 = 7$ T. The field is in the (a^*c) -plane, and the polar angle, θ , is reckoned from \vec{a}^* direction towards $[00\bar{1}]$.

Figure 3. Angular evolution of ^1H NMR spectrum in the (a^*c) plane measured at 74 K in field $H_0=7$ T. Circles are the measured peak positions. Lines are model calculations using Equation 1.



To model the observed proton spectrum one needs to sum up the dipolar fields, h_{dip} , created at the nucleus site by Mn^{2+} electronic spins, and take into account the sample geometry resulting in a demagnetizing field, h_{D} , and the Lorentz field, h_{Lor} , which is the mean field induced at the nucleus site by the bulk of the sample located outside the dipolar summation sphere [13].

For the magnetic field in the (a^*c)-plane, $\vec{H} = [H_0 \cos \theta, 0, H_0 \sin \theta]$ we model the spectrum as

$$\nu - \nu_0 = \gamma_n \left(\sum_i h_{\text{dip}}^i + h_{\text{Lor}} - h_{\text{D}} \right) \quad (1a)$$

$$h_{\text{dip}}^i = \mu_{\text{Mn}} \frac{3 \cos^2 \alpha_i - 1}{r_i^3} \quad (1b)$$

$$h_{\text{Lor}} = \frac{4\pi}{3} \frac{\mu_{\text{Mn}}}{V_{\text{Mn}}}, \quad h_{\text{D}} = 4\pi N \frac{\mu_{\text{Mn}}}{V_{\text{Mn}}} \quad (1c)$$

Here, $\gamma_n = ^1\gamma$; μ_{Mn} is the thermal average of the Mn^{2+} magnetic moment projection on the field direction, r_i is the length of the position vector from the proton site to the Mn site i , α_i is the angle between this vector and the field direction, V_{Mn} is the unit cell volume per Mn^{2+} ion, and $N = N_{\perp} \cos^2 \theta + N_{\parallel} \sin^2 \theta$ is the demagnetization factor.

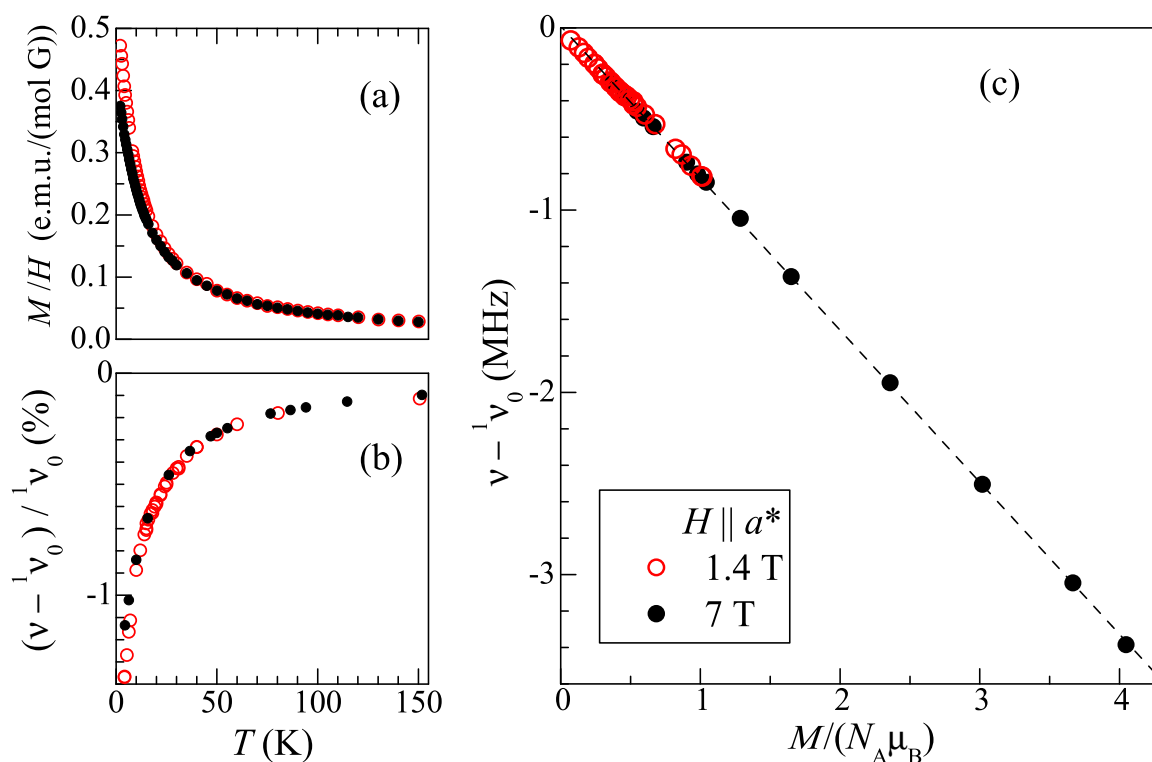
Since the DC magnetization in $\kappa\text{-(BETS)}_2\text{Mn}[\text{N}(\text{CN})_2]_3$ is determined by Mn^{2+} magnetic moments [3], we put in Equation 1 $\mu_{\text{Mn}} = M/N_A$, where M is the measured DC magnetization per mole (3800 emu/mol at $H_0 = 7$ T, $T = 74$ K) and N_A is Avogadro's number. For our very thin-plate sample we assume the demagnetization factors $N_{\perp} = 1$, $N_{\parallel} = 0$. Crystallographic positions of Mn and

H atoms required to calculate Equation 1b are available online from the CCDC library as mentioned in the Experimental Section. The sum in Equation 1a has been taken over ~ 200 Mn sites within ± 20 Å to provide reasonable convergence.

The peak positions calculated using Equation 1 for each of the 8 inequivalent hydrogen sites are shown in Figure 3 by solid lines. The agreement between the calculated and the measured peak positions is clearly reasonable despite the absence of any fit parameters used in the calculations. This indicates that ^1H NMR frequency shift is determined by the dipolar fields from Mn^{2+} at the hydrogen site, at least at this field and temperature.

To check if this is true for all temperatures, we compare the temperature dependences of the DC magnetization and the ^1H NMR peak positions. Figure 4a,b show temperature dependences of, respectively, the molar DC magnetization normalized to the applied field, M/H , and the normalized frequency shift of the lowest-frequency peak in the spectrum measured in $H \parallel a^*$ geometry ($\theta = 0$ in Figure 3), for the magnetic fields 1.4 and 7 T.

Figure 4. (a) Molar magnetization vs. temperature in $H = 1.4$ and 7 T; (b) Position of the lowest-frequency peak in ^1H NMR spectrum in $\vec{H} \parallel \vec{a}^*$ geometry vs. temperature in $H = 1.4$ and 7 T; (c) Position of the peak for the temperature range 4–150 K, in function of the DC magnetization per Mn ion, $\mu_{\text{Mn}} = M/N_A$, measured at the same temperatures and fields and expressed in terms of the Bohr magneton, μ_B . Open red circles and closed black circles correspond to the fields 1.4 and 7 T, respectively.

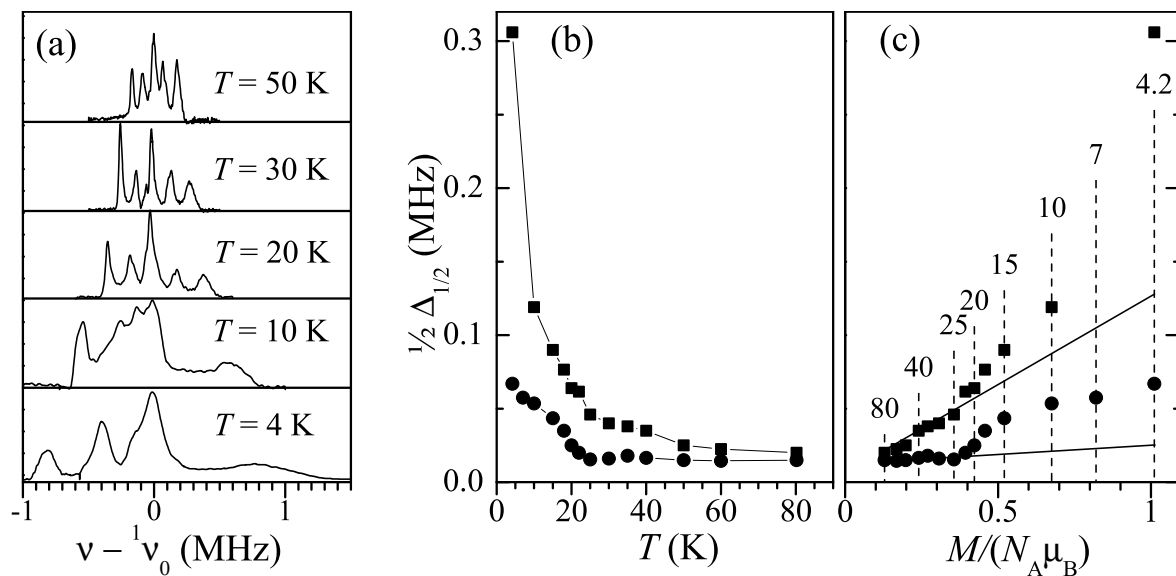


The right panel of Figure 4 depicts the plot of the proton frequency shift, $\nu - \nu_0$, in function of the magnetization measured at the same temperatures and fields. The linearity of the data in Figure 4 demonstrates that for the whole temperature and field ranges covered in the experiment, the positions

of ^1H NMR spectrum peaks are determined by the magnetic subsystem associated with Mn^{2+} moments, and can be utilized as Hall probes of the Mn^{2+} dipolar fields at hydrogen sites.

Figure 5a shows the evolution of ^1H NMR spectrum ($H_0 = 1.4\text{ T}$ parallel to \vec{a}^*) with temperature. As can be seen, the frequency span of the spectrum increases with decreasing temperature while its shape is maintained down to $\sim 20\text{ K}$. At lower temperature the peaks broaden rapidly, which is more pronounced on the right-hand side of the spectrum. Figure 5b depicts the temperature dependence of the half width at half height, $\frac{1}{2}\Delta_{1/2}$, for the leftmost and the rightmost peaks in the spectrum. As one can see in Figure 5, the linewidth is relatively flat above $T_{\text{MI}} \approx 23\text{ K}$ (especially for the leftmost peak) and increases sharply below this temperature. Figure 5c demonstrates the plot of the linewidths in function of the DC magnetization. One can see in Figure 5c a crossover in the linewidth behavior at T_{MI} which is observed as an upturn from the linear M -dependence (shown by solid lines) obeyed at higher temperatures.

Figure 5. (a) Temperature evolution of ^1H NMR spectrum measured at $H_0 = 1.4\text{ T}$ parallel to \vec{a}^* ; (b) Temperature dependence of the half-linewidth of the leftmost (circles) and the rightmost (squares) peaks; (c) The leftmost and the rightmost peak half-linewidths in function of the DC magnetization. Solid lines extrapolate the linewidth behavior above 25 K to low temperatures. Dashed lines with numbers on top mark measurement temperatures.



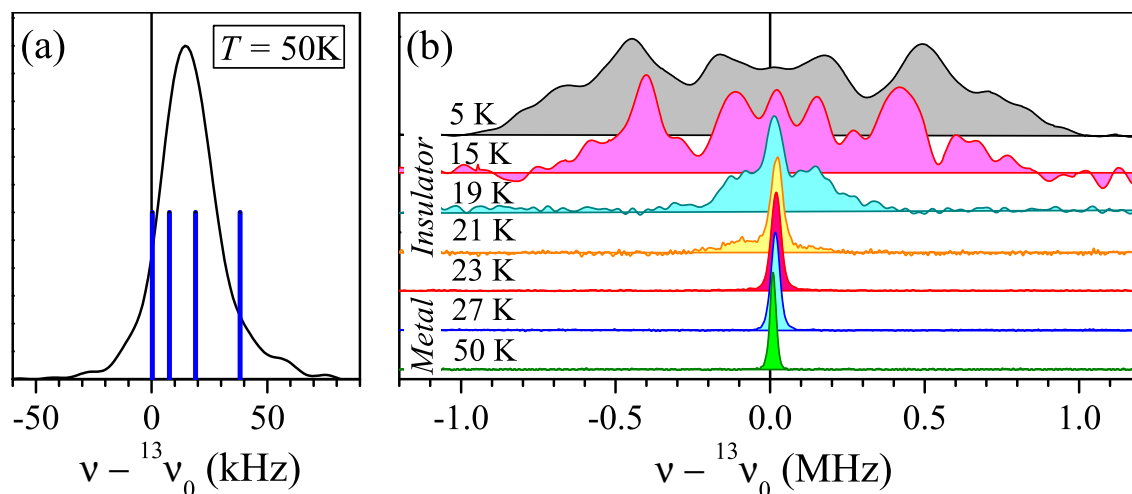
Since the ^1H NMR peak positions are highly anisotropic as can be seen in Figure 3, there is a number of trivial reasons for the peaks to be broadened, including sample imperfections on the macroscopic and local levels, as well as minor misalignment of the magnetic field from \vec{a}^* direction, as discussed in [14]. However, all of them should make the linewidth as linear in the magnetization as the peak position itself is (Figure 4c). The upturn of the linewidth M -dependence below $T_{\text{MI}} \approx 23\text{ K}$ (Figure 5c) indicates the onset of yet another broadening mechanism. Provided that the crystal lattice is intact, this should be related with local-level scatter of the dipolar fields from Mn^{2+} at the hydrogen site, for example, a variable from site to site tilt of the Mn^{2+} static moments. This site variation of the tilt is apparently random or incommensurate with the crystal lattice, because otherwise a splitting of ^1H NMR peaks would take place instead of the featureless broadening observed in the experiment (Figure 5a). The tilt

of the Mn^{2+} moments emerging below T_{MI} , together with the deviation of the magnetization from the Curie–Weiss behavior [3], indicates apparently the tendency of the Mn^{2+} spin system towards the AF order. Frustrated geometrically by triangular arrangement of Mn in the anion layer (Figure 1e), Mn^{2+} system is resolved into a disordered (like spin-glass) or an incommensurate spin structure.

2.2. ^{13}C NMR

The ^{13}C NMR spectra were measured in $\kappa\text{-(BETS)}_2\text{Mn[N(CN)}_2\text{]}_3$ in the external field $H = 7$ T aligned perpendicular to $[0\bar{1}1]$ at 45° to \bar{a}^* . For this experimental geometry, the metallic-state spectrum in theory is represented by four peaks arising from the two magnetically different orientations of the BETS dimers (Figure 1c) and nonequivalent (“inner” and “outer”) carbon sites of the central C=C bond within the dimer (Figure 1d) [15]. The dipolar interaction between ^{13}C spins in the C=C bond, which in general provides another factor of two to the number of peaks, is nearly zero for this field orientation.

Figure 6. ^{13}C NMR spectra measured in the external field $H = 7$ T aligned perpendicular to $[0\bar{1}1]$ at 45° to \bar{a}^* . The spectra are shown with respect to $^{13}\nu_0 = 74.946$ MHz. (a) The spectrum at $T = 50$ K. Blue solid lines indicate positions of the resonance peaks calculated with the shift tensor of $\kappa\text{-(ET)}_2\text{Cu[N(CN)}_2\text{]Br}$ [15]; (b) The evolution of the ^{13}C NMR spectrum with temperature.



Unlike the magnetic ion-free quasi-two-dimensional ET-based conductors where the NMR peaks from magnetically nonequivalent ^{13}C sites are usually well resolved, ^{13}C spectrum in the metallic state of $\kappa\text{-(BETS)}_2\text{Mn[N(CN)}_2\text{]}_3$ for this field orientation is represented by a single featureless Gaussian-shaped line. The left panel in Figure 6 represents the spectrum taken at $T = 50$ K. Using the ^{13}C NMR shift tensors obtained for $\kappa\text{-(ET)}_2\text{Cu[N(CN)}_2\text{]Br}$ [15] (which is nearly the same as for $\kappa\text{-(ET)}_2\text{Cu[N(CN)}_2\text{]Cl}$ [16]), for the given experimental geometry one expects a $\kappa\text{-(BETS)}_2\text{Mn[N(CN)}_2\text{]}_3$ sample to produce the resonance peaks at 2.7, 10.7, 22.7, and 40.8 kHz (with respect to $^{13}\nu_0 = 74.946$ MHz). Dipolar fields from Mn^{2+} moments provide additional shifts to the resonance frequencies, which can be calculated following Equations 1 using the values of Mn^{2+} moments known from the bulk magnetization measurements [3]. At $T = 50$ K the calculated dipolar fields from Mn^{2+} move the listed peaks to positions at 0.3, 7.7, 19, and 38.2 kHz. The calculated peak positions are

shown by vertical lines in Figure 6a. One can see that the spectrum measured at 50 K covers fairly well the range of the calculated peak positions indicating that the ^{13}C shift tensor in the title compound is not much different from that in $\kappa\text{-(ET)}_2\text{Cu[N(CN)}_2\text{]Br}$.

Evidently, the peaks from individual carbon sites in the metallic state of $\kappa\text{-(BETS)}_2\text{Mn[N(CN)}_2\text{]}_3$ are vastly broadened that merges them into a single line. Some broadening of ^{13}C NMR peaks has been noticed in $\kappa\text{-(ET)}_2\text{Cu[N(CN)}_2\text{]Br}$ and a number of reasons has been recruited to explain it [15], including spacial variation of the π -electron spin density due to precursors to Anderson localization or spin-density wave. For the sample reported here, the linewidth is expected broader than in non-magnetic compounds due to the presence of the anisotropic dipolar fields from Mn^{2+} . For example, the same mechanism that creates the ^1H NMR linewidth (Figure 5b) will be responsible for ~ 10 kHz linewidth of the ^{13}C peaks at carbon sites at 50 K. Anyway, more detailed analysis of the possible broadening mechanisms in the metallic state is beyond the scope of this communication.

The right panel in Figure 6 demonstrates the evolution of the ^{13}C NMR spectrum with temperature. The single peak characteristic of the spectrum in the metallic state above $T = 23\text{ K} \approx T_{\text{MI}}$ develops below this temperature into a broad symmetric pattern counting 5 pronounced peaks. Below $T = 15\text{ K}$ the spectrum spans the range of nearly ± 1 MHz, which is huge compared to the spectrum width in the metallic state. This cannot result from the dipolar fields created by Mn^{2+} : calculations show that fully polarized Mn^{2+} can provide a dipolar shift ranging from -12.5 to -19 kHz (depending on the carbon site) in 7 T field. Therefore the spectrum in the insulating state evidences enhancement of the electron spin density at carbon sites due to electron spins localized on the dimers of the BETS molecules. Moreover, several pronounced peaks are visible in the low-temperature spectrum, which infers a commensurate order of the localized spins. Finally, the symmetric shape of the spectrum indicates the staggered order, because antiparallel components of the staggered electron spins ($\hat{\mathbf{S}}_i = -\hat{\mathbf{S}}_j$) produce opposite local fields at carbon sites i and j : $h_i = \hat{\mathbf{I}}_i \cdot \mathbf{A} \cdot \hat{\mathbf{S}}_i = -(\hat{\mathbf{I}}_j \cdot \mathbf{A} \cdot \hat{\mathbf{S}}_j) = -h_j$, where $\hat{\mathbf{I}}$ and $\hat{\mathbf{S}}$ are the nuclear and electron spin operators, respectively, and \mathbf{A} is the hyperfine tensor. In turn, this signifies the AF exchange interaction between the localized spins. The staggered component of the spin magnetization lies apparently somewhere in the plane perpendicular to the magnetic field, since the anisotropic AF exchange term is usually much smaller than 7 T, the external field of this experiment.

The frequency range of the ^{13}C spectrum in $\kappa\text{-(BETS)}_2\text{Mn[N(CN)}_2\text{]}_3$ at $T = 5\text{ K}$ (Figure 6b) is of the same order of magnitude ($\sim \pm 1$ MHz) as observed in the AF state of $\kappa\text{-(ET)}_2\text{Cu[N(CN)}_2\text{]Cl}$ [16] and $\beta'\text{-(ET)}_2\text{ICl}_2$ [17]. The magnitude of the electron spin magnetization of $0.5 \mu_{\text{B}}$ and $1 \mu_{\text{B}}$ per dimer, respectively, has been reported for these two compounds. Therefore in $\kappa\text{-(BETS)}_2\text{Mn[N(CN)}_2\text{]}_3$ this value should be within the same range since the hyperfine tensor here is expected to be similar, as the measurements in the metallic phase suggest.

More detailed and quantitative information about the spin structure of the localized π electrons can hardly be derived at the moment. To do this one needs to know more or less exactly the hyperfine tensors for the central carbons in $\kappa\text{-(BETS)}_2\text{Mn[N(CN)}_2\text{]}_3$, which in turn requires the value of the π spin susceptibility never reported so far (but probably accessible via ESR).

3. Experimental

The crystal structure of κ -(BETS)₂Mn[N(CN)₂]₃ is monoclinic with the space group $P2_1/c$ and the lattice constants at 88 K $a = 19.428 \text{ \AA}$, $b = 8.379 \text{ \AA}$, $c = 11.869 \text{ \AA}$, $\beta = 92.67^\circ$, and $V = 1930.1 \text{ \AA}^3$, with two formula units per unit cell. The conducting layers formed by BETS dimers in the (bc) plane are sandwiched between the polymeric Mn[N(CN)₂]₃ anion layers in the a direction (Figure 1a). The crystal structure is available at Cambridge Crystallographic Data Centre [18], CCDC 775974-775977, and has been discussed in details in earlier communications [1,2].

Crystals for ¹H NMR (with all natural-abundant carbon) were obtained by electrochemical oxidation of BETS in the mixture of solvents, 1,1,2-trichloroethane/ethanol (10:1 v/v), in the presence of Mn[N(CN)₂]₂ as electrolyte [1,2]. The ¹³C-enriched samples were synthesized by electrochemical oxidation of ¹³C-labeled BETS in benzonitrile/ethanol (10:1 v/v) in the presence of Ph₄PMn[N(CN)₂]₃ complex salt as electrolyte following the procedure reported in Reference [19]. ¹³C-enriched (>99%) BETS (Figure 1b) was synthesized with the use of ¹³C-enriched triphosgene (*bis*(trichloromethyl-¹³C₃)carbonate) according to the method described in literature [20].

The single crystals used in the ¹H NMR experiments had the dimensions $a^* \times b \times c \sim 0.05 \times 3 \times 1 \text{ mm}^3$. The dimensions of the crystal for ¹³C NMR were $\sim 0.05 \times 3 \times 3 \text{ mm}^3$. Crystallographic orientations of the crystals were X-ray defined. NMR spectra were acquired using standard spin-echo sequence with π -pulse length $\leq 2.5\text{--}3 \mu\text{s}$. To cover broad spectra, Fourier-transforms of the acquired spin-echoes were collected at 150 kHz intervals and summed up.

4. Conclusions

We performed ¹H and ¹³C NMR measurements in κ -(BETS)₂Mn[N(CN)₂]₃ to find the relation between the MI transition and the properties of the spin systems of the localized $3d \text{ Mn}^{2+}$ ions and the conduction π electrons. We found that transition of the system into the insulating state is followed by localization of the π spins into a long-range ordered staggered structure of AF type. It should be emphasized here that this structure does not necessarily signify the conventional AF state but can be a field-induced effect in the presence of the Dzyaloshinskii–Moriya interaction, as it happens in κ -(ET)₂Cu[N(CN)₂]Cl [21].

In contrast, the Mn^{2+} spins do not order below T_{MI} but are likely to form a disordered tilted structure, which may signify their trend to AF order, frustrated geometrically by the triangular arrangement of Mn in the anion layer.

Our findings show that the MI transition in κ -(BETS)₂Mn[N(CN)₂]₃ is not the consequence of the interactions within the $3d \text{ Mn}^{2+}$ electron spin system transferred to the conduction spin system by the π - d coupling, but is a result of the interactions within the π -electron system itself as in some magnetic ion-free quasi-two-dimensional charge-transfer salts. Vice versa, the observed formation of the disordered tilted structure in the Mn^{2+} electron spin system could be induced by the π -spin ordering via the π - d interaction. It has been reported in [3] that the susceptibility of κ -(BETS)₂Mn[N(CN)₂]₃ determined by the Mn^{2+} spin system depends on temperature as $1/(T + \theta)$ with $\theta \approx 5.5 \text{ K}$. That means that the Mn^{2+} subsystem should remain paramagnetic down to $T \sim \theta$, while in fact it deviates from the paramagnetic

state at higher temperature $T_{MI} \sim 23$ K, suggesting the influence of the spin-ordered localization of π -electrons.

Acknowledgements

The authors gratefully acknowledge fruitful suggestions from S. E. Brown, assistance in the questions of crystallography from S. S. Khasanov, and technical support from N. A. Belov. This work was supported by the RFBR grants 10-02-01202 and 11-02-91338-DFG (DFG grant Bi 340/3-1), Russian State Contract 14.740.11.0911, and the Program of Russian Academy of Sciences. This work was partially supported by Grant-in-Aid for Scientific Research (S) (No. 22224006) from the Japan Society for the Promotion of Science (JSPS).

References

1. Zverev, V.N.; Kartsovnik, M.V.; Biberacher, W.; Khasanov, S.S.; Shibaeva, R.P.; Ouahab, L.; Toupet, L.; Kushch, N.D.; Yagubskii, E.B.; Canadell, E. Temperature-pressure phase diagram and electronic properties of the organic metal κ -(BETS)₂Mn[N(CN)₂]₃[N(CN)₂]₃. *Phys. Rev. B* **2010**, *82*, 155123:1–155123:9.
2. Kushch, N.D.; Yagubskii, E.B.; Kartsovnik, M.V.; Buravov, L.I.; Dubrovskii, A.D.; Chekhlov, A.N.; Biberacher, W. π -Donor BETS based bifunctional superconductor with polymeric dicyanamidomanganate(II) anion layer: κ -(BETS)₂Mn[N(CN)₂]₃[N(CN)₂]₃. *J. Am. Chem. Soc.* **2008**, *130*, 7238–7240.
3. Vyaselev, O.M.; Kartsovnik, M.V.; Biberacher, W.; Zorina, L.V.; Kushch, N.D.; Yagubskii, E.B. Magnetic transformations in the organic conductor κ -(BETS)₂Mn[N(CN)₂]₃[N(CN)₂]₃ at the metal-insulator transition. *Phys. Rev. B* **2011**, *83*, 094425:1–094425:6.
4. Brossard, L.; Clerac, R.; Coulon, C.; Tokumoto, M.; Ziman, T.; Petrov, D.K.; Laukhin, V.N.; Naughton, M.J.; Audouard, A.; Goze, F.; *et al.* Interplay between chains of $S = 5/2$ localised spins and two-dimensional sheets of organic donors in the synthetically built magnetic multilayer λ -(BETS)₂FeCl₄. *Eur. Phys. J. B* **1998**, *1*, 439–452.
5. Uji, S.; Brooks, J.S. Magnetic-field-induced superconductivity in organic conductors. *J. Phys. Soc. Jpn.* **2006**, *75*, 051014:1–051014:10.
6. Kagawa, F.; Miyagawa, K.; Kanoda, K. Magnetic Mott criticality in a κ -type organic salt probed by NMR. *Nat. Phys.* **2009**, *5*, 880–884.
7. Welp, U.; Fleshler, S.; Kwok, W.K.; Crabtree, G.W.; Carlson, K.D.; Wang, H.H.; Geiser, U.; Williams, J.M.; Hitsman, V.M. Weak ferromagnetism in κ -(ET)₂Cu[N(CN)₂]Cl, where (ET) is *bis*-(ethylenedithio)tetrathiafulvalene. *Phys. Rev. Lett.* **1992**, *69*, 840–843.
8. Yoneyama, N.; Miyazaki, A.; Enoki, T.; Saito, G. Magnetic properties of (BEDT-TTF)₂X with localized spins. *Synth. Met.* **1997**, *86*, 2029–2030.
9. Akiba, H.; Nakano, S.; Nishio, Y.; Kajita, K.; Zhou, B.; Kobayashi, A.; Kobayashi, H. Mysterious paramagnetic states of Fe 3d spin in antiferromagnetic insulator of κ -BETS₂FeCl₄ system. *J. Phys. Soc. Jpn.* **2009**, *78*, 033601:1–033601:3.

10. Waerenborgh, J.C.; Rabaça, S.; Almeida, M.; Lopes, E.B.; Kobayashi, A.; Zhou, B.; Brooks, J.S. Mössbauer spectroscopy and magnetic transition of κ -(BETS)₂FeCl₄. *Phys. Rev. B* **2010**, *81*, 060413:1–060413:4.
11. Klutz, T.; Hennig, I.; Haebleren, U.; Schweitzer, D. Knight shift tensors and π -spin densities in the organic metals α _t-(BEDT-TTF)₂I₃ and (BEDT-TTF)₂Cu(NCS)₂. *Appl. Mag. Res.* **1991**, *2*, 441–463.
12. Kanoda, K. Recent progress in NMR studies on organic conductors. *Hyperfine Interact.* **1997**, *104*, 235–249.
13. Uritskii, M.; Irkhin, V. Calculation of dipole fields at interstices of rare-earth metals. *Phys. Solid State* **2000**, *42*, 399–405; *Fizika Tverdogo Tela* **2000**, *42*, 390–396.
14. Vyaselev, O.M.; Kushch, N.D.; Yagubskii, E.B. Proton NMR study of the organic metal κ -(BETS)₂Mn[N(CN)₂]₃[N(CN)₂]₃. *J. Exp. Theor. Phys.* **2011**, *113*, 835–841; *Zh. Eksp. Teor. Fiz.* **2011**, *140*, 961–967.
15. de Soto, S.M.; Slichter, C.P.; Kini, A.M.; Wang, H.H.; Geiser, U.; Williams, J.M. ¹³C NMR studies of the normal and superconducting states of the organic superconductor κ -(ET)₂Cu[N(CN)₂]Br. *Phys. Rev. B* **1995**, *52*, 10364–10368.
16. Smith, D.F.; de Soto, S.M.; Slichter, C.P.; Schlueter, J.A.; Kini, A.M.; Daugherty, R.G. Dzialoshinskii-Moriya interaction in the organic superconductor κ -(BEDT-TTF)₂Cu(N[CN]₂)Cl. *Phys. Rev. B* **2003**, *68*, 024512:1–024512:9.
17. Eto, Y.; Kawamoto, A. Antiferromagnetic phase in β' -(BEDT-TTF)₂ICl₂ under pressure as seen via ¹³C NMR. *Phys. Rev. B* **2010** *81*, 020512:1–020512:4.
18. Cambridge Crystallographic Data Centre. http://www.ccdc.cam.ac.uk/data_request/cif (accessed on 10 April 2012).
19. Kushch, N.D.; Buravov, L.I.; Chekhlov, A.N.; Spitsina, N.G.; Kushch, P.P.; Yagubskii, E.B.; Herdtweck, E.; Kobayashi, A. The first BETS radical cation salts with dicyanamide anion: Crystal growth, structure and conductivity study. *J. Solid State Chem.* **2011**, *184*, 3074–3079.
20. Kato, R.; Kobayashi, H.; Kobayashi, A. Synthesis and properties of bis(ethylenedithio) tetraselenafulvalene (BEDT-TSeF) compounds. *Synth. Met.* **1991**, *42*, 2093–2096.
21. Kagawa, F.; Kurosaki, Y.; Miyagawa, K.; Kanoda, K. Field-induced staggered magnetic moment in the quasi-two-dimensional organic Mott insulator κ -(BEDT-TTF)₂Cu[N(CN)₂]Cl. *Phys. Rev. B* **2008**, *78*, 184402:1–184402:10.